Progress in Propulsion Physics **2** (2011) 641-654

EXPERIMENTAL STUDY OF A PLANAR EXPANSION–DEFLECTION NOZZLE

B. Wagner, R. Stark, and S. Schlechtriem

Institute of Space Propulsion
German Aerospace Center
Lampoldshausen, Hardthausen 74239, Germany

A planar expansion–deflection (ED) nozzle was tested in the cold-flow P6.2 test bench at German Aerospace Center (DLR) Lampoldshausen. The comparison between design, experimental data, and numerical results at the design point of $p_0/p_a = 30$ shows, in general, a good agreement with slight discrepancy due to a higher expansion in the experiments. The center-body base wake closure was studied from transient pressure profiles ($p_0/p_a = 15$–25). A hysteresis was shown to exist in the transition from the open to the closed wake mode and back. For low-pressure ratios ($p_0/p_a = 6$, i. e., off-design operation), flow separation on the center body occurred. The related separation shock was shown to interact with the opposite outer contour leading to pressure peaks.

1 INTRODUCTION

In the early 1960s, the research on alternative nozzle concepts capable of adapting to the ambient pressure was launched. At this time, the ED nozzle concept was developed [1]. The ED nozzle seemed to be a promising idea due to a free boundary inside the nozzle. However, for different reasons, e. g., the altitude compensation was in doubt [2], the ED nozzle concept was not further considered for rocket main engine applications.

Nowadays, the ED concept is again under consideration to be applied for the upper-stage engines [3]. A shorter nozzle length could lead to mass saving at a comparable performance, especially if the combustion chamber is integrated into the nozzle. Thus, the injection direction in the combustion chamber is reverse to the outflow direction at the nozzle exit. Furthermore, expander-cycle type engines could benefit from the increased heat transfer at the large surface areas and the elongated throat region, typically the region with the highest heat transfer [4].

Recently detailed analytical and numerical studies of the flow behavior and the performance of an ED nozzle have been made for both atmospheric flight and vacuum conditions [5]. Numerical methods, e. g., for the sonic line evaluation, have been combined with the method of characteristics (MOC) for the flow field calculation [6]. The shape of the sonic line influences the starting line of the MOC and, hence, the entire nozzle design. Simple analytical studies for conventional nozzles, as, e. g., Sauer [7], are not suitable for throat modeling in the ED nozzle due to the flow passing an inclined throat, without a clear dominant velocity vector. Numerical approaches to estimate the sonic line seem to be the only feasible way, but the results need experimental validation.

The center body with the viscous flow region at its base is another critical flow region to design as the MOC is limited to the supersonic flow field. Additional methods must be used to predict the base pressure as it has an impact on the overall performance of the nozzle. The transition from the open to the closed wake mode is also excluded from the MOC design. Computational fluid analysis can support the design process, but for reliability, they need to be validated.

Therefore, an ED nozzle test program was started at DLR Lampoldshausen to verify the existing design tools and to build a database for CFD validation. A generic planar nozzle was designed in order to study the two critical design regions, the throat and the center body wake. The ED nozzle was kept planar for the use of optical diagnostics and pressure measurements within these zones. The first studied nozzle had parallel inflow and outflow directions, but the pintle was already extended to a center body as this would be the case for a reverse-flow ED nozzle where the combustion chamber will be integrated into the supersonic flow field.

2 FLOW FIELD DESCRIPTION

The flow field inside an ED nozzle can be divided into two operational modes which depend on the pressure ratio of total to ambient pressure. At very low ambient pressures or vacuum conditions, thus at high pressure ratios, the nozzle operates in the closed wake mode. The flow expands along the center body and detaches globally at its end. The boundary layer separates and continues as a part of the shear layer between the supersonic nozzle flow and the subsonic flow region downstream the center body. The wake flow in the base region is trapped by the inner shear layer and no reaction on the ambience is possible. As a result, the shearing forces lead to a closed recirculation. Since the supersonic flow deflected by the expansion must be redirected parallel to the centerline, a shock wave is generated where the shear layer reattaches and turns towards the centerline. Under sea level conditions, the closed wake mode can also be obtained at a sufficiently high supply pressure. This is the case for the presented

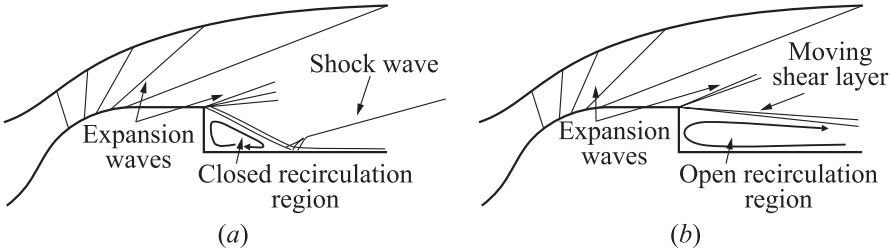

Figure 1 Flow features inside the tested ED nozzle: closed (*a*) and open (*b*) wake modes

configuration (Fig. 1*a*). The flow near the contoured upper wall is expanded to sea level pressure and the flow along the center body is further expanded around the pintle corner towards the centerline. So, at the nozzle exit, three pressure regions can be found: adapted pressure near the upper contour wall, higher pressure near the centreline behind the deflecting shock, and lower pressure in between.

At lower pressure ratios, a wake closure is not achieved. The shear layer in this case acts as a free boundary between the supersonic flow and the viscous open recirculation zone, which is now reacting on the ambient pressure. The shear layer moves towards the centerline with increasing the nozzle pressure ratio and *vice versa*. The aspiration effect of the shear layer causes a lower than ambient pressure value in the base region. This flow condition is called the open wake mode (Fig. 1*b*).

3 EXPERIMENTAL SETUP

3.1 Test Bench

The cold-gas subscale P6.2 test facility [8] at the DLR Lampoldshausen was used for the presented experiments. The test bench consists of two test positions, a closed high-altitude simulation chamber [9], and a horizontal test position under ambient conditions. Blowdown tests against ambient pressure with a maximum feeding pressure of 3 MPa were performed (see flow plan, Fig. 2*a*). The fluid, dry nitrogen, is stored in 7 high-pressure vessels at 20 MPa under ambient temperature conditions. Due to the large mass flow during the experiments, all vessels were joined to provide sufficient primary pressure. After passing the hand valves and the automatic valve, the nitrogen is cleaned from small particles in a high pressure filter before entering the pressure regulator. Finally, the test specimen's feeding pressure is controlled by the fraction of total opening of the control valve. A high accuracy in both nominal values and repeatability is

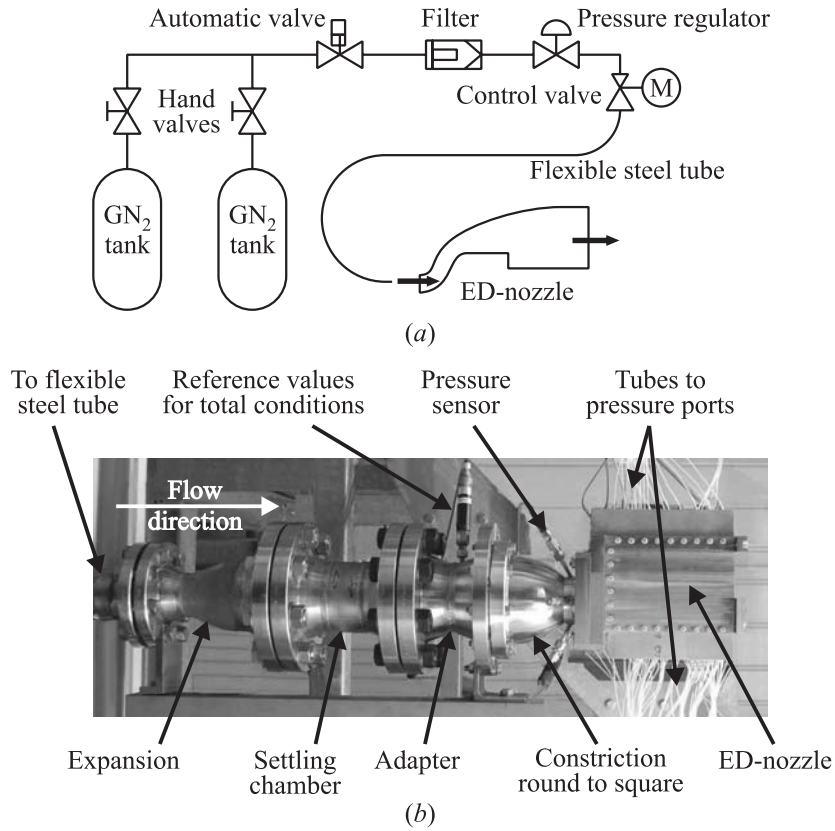

Figure 2 Integration of the experimental setup into P6.2 test bench: (*a*) sketch of the 4 MPa feeding system; and (*b*) picture of the horizontal setup

achieved. The flow rate is measured by the pressure drop of a calibrated orifice disc downstream of the control valve.

After the flexible steel tube, the flow is expanded to the largest cross section in the setup, which is $12.8A_t$ where A_t is the area corresponding to the nozzle throat. At this location, with the lowest flow velocity, the settling chamber is placed. It consists of a honeycomb structure of a tube size of 3.5 mm and three meshes with a mesh size of 2 mm. A plenum is attached to the settling chamber, with an equal diameter. The total pressure (p_0) and the total temperature are measured here (Fig. 2*b*) and are taken as reference values.

The following constriction to the nozzle inlet is carried out simultaneously with the transition from a round to a square cross section. In order to provide a homogeneous flow field, this constriction contour was designed as a wind tunnel

constriction proposed by Börger [10]. This method minimizes the length of the constriction for a given constriction ratio, avoiding flow separation and leading to a homogeneous subsonic flow field at the exit while using a 5th order equation approach. The component was built from one piece by eroding the inner contour with several copper electrodes.

3.2 Nozzle

Although planar nozzles are unlikely to be used in rocket propulsion, they benefit from a good access for measurement techniques, especially for optical diagnostics, e. g., Schlieren visualization. A drawback of a planar setup are the corner effects and the difficulties in manufacturing and sealing. By laser welding of the two nozzle parts into the flange frame, these problems could be solved, while keeping access to the flow field through removable side walls. Instead of a symmetric nozzle, only one half of an ED nozzle was designed. This increases the throat section for measurement applications at a given maximum mass flow, which is limited by the test bench. The symmetry line, which would normally be downstream the center body, is substituted by a solid wall. This part can also be equipped with pressure ports.

The nozzle inflow is given by the square cross section of the constriction with a width of $2.5G_t$ where G_t is the smallest distance between the upper contour and the lower pintle wall. The duct span of the nozzle is $2.5G_t$, too. Details of the throat section can be found in Fig. 3*a*. The throat design is comparable to the model proposed by Taylor and Hempsell [6], omitting the contour circular arc downstream G_t and with a simpler pintle shape.

The contour is designed for $p_2/p_a = 1.8$ at the end of the center body (see position 2 in Fig. 3*a*) where p_a is the ambient pressure. The pressure ratio was chosen to assure a wake closure for $p_0/p_a = 30$, without uncertainties. The

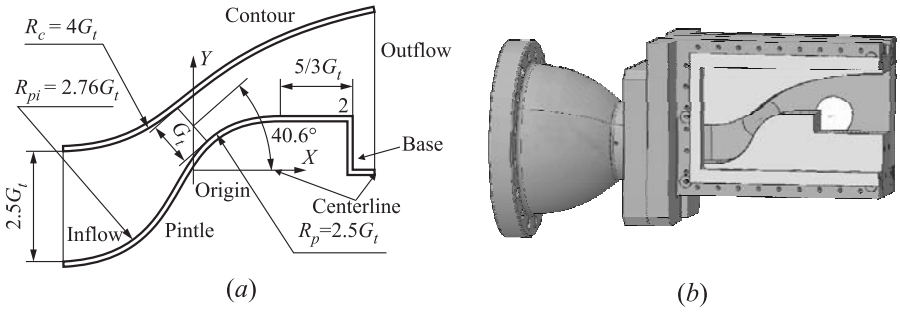

Figure 3 Tested planar ED nozzle: (*a*) throat region in detail; and (*b*) CAD model of the nozzle attached to the constriction. Positions of the Schlieren windows are indicated

actual transition point was a part of the experimental study. As a guideline for the dimensioning, the experiments of Mueller [11] were considered, where a wake closure was achieved for $p_2/p_a = 1.63$.

The exit conditions of the nozzle are given by an expansion to the ambient pressure at sea level. The wall contour is designed by a Prandtl–Meyer expansion resulting in an area ratio of 4. With the given boundary conditions, it was not possible to keep the inflow line and the centerline of the pintle on the same level. The defined X-axis is identical with the centerline downstream the center body. Its origin is located at the intersection of the elongated centerline and a line through the middle of the smallest gap between upper contour and pintle wall, as it can be seen in Fig. 3*a*. The flow direction in the throat is 40.6° inclined to the X-axis. As the inflow and the outflow direction is the same, this setup is called the linear flow configuration. Two other configurations, one of them as a reverse-flow nozzle, are planned. The throat region was designed to fit those future configurations, too.

The new in this design is the extended center body. Near the pintle wall the expansion ends at the end of the circular contour after the throat. The pintle was elongated by $5/3G_t$ parallel to the centerline where no further expansion takes place. The center body shape is derived from the design of a reverse-flow nozzle with a combustion chamber integrated into the nozzle. This configuration leads to a conical body in the supersonic flow region [3].

3.3 Data Acquisition

All wall pressure orifices (0.5 mm) were connected with steel tubes, which were laser welded into the outer nozzle walls. Those tubes were joined through Teflon pipes with an interface block in which the pressure sensors were mounted. To ease the mounting of the setup, the pipes were chained with Quick-Disconnects. Thirty-four pressure sensors with a maximum operating pressure of 0.07 to 5 MPa were used, mostly Kulite (XT-154-190M) and some Kistler (4043) sensors. The measuring precision was 0.1%, related to the maximum operating pressure.

The signals from the pressure sensors were amplified with in-house developed AS2 amplifiers and filtered with a low-pass cutoff frequency of 160 Hz. The data were stored with a sampling rate of 1 kHz. For successive test campaigns, high-frequency channels can be used, with a sampling rate up to 100 kHz.

The pressure sensors were calibrated statically prior the campaign. An offset correction was done before each test run, relative to the ambient pressure.

3.4 Test Profile

Three types of total pressure profiles were considered, from which the test sequences have been derived. Each type of the profile covered a typical flow be-

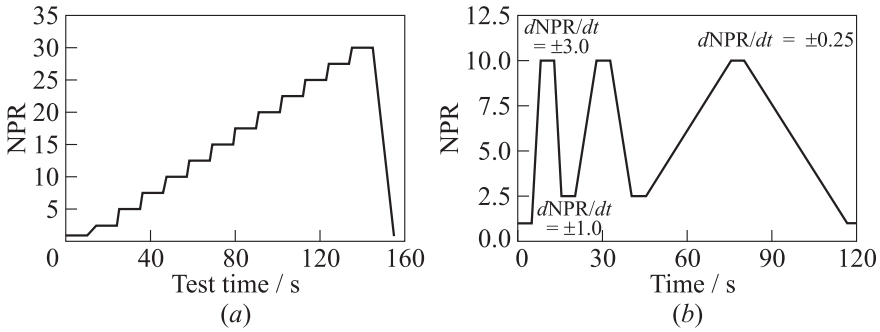

Figure 4 Examples of test profiles: (*a*) with stationary plateaus; and (*b*) with transient ramps

havior of the ED nozzle. For easier comparison, the nozzle pressure ratio (NPR) was used for the ratio of total-to-ambient pressure (p_0/p_a). The first profile was an up-ramping profile with stationary plateaus for each NPR = 2.5 step (Fig. 4*a*). On the plateaus, mean data values could be obtained gaining the stationary wall and base pressure distribution. With the second test profile, the transition behavior and the wake closure of the nozzle in the corresponding pressure region (NPR = 15–25) could be studied. For this purpose, transient tests with two different pressure gradients, $d\text{NPR}/dt = 2.5$ and 0.5, respectively, were performed. The third profile varied the supply pressure in the low-pressure region NPR = 2.5–10 as the flow behavior at the off-design was of interest (Fig. 4*b*). Due to the blowdown character of the tests, the total temperature decreased during the tests. Depending on the mass flow and the test length, the total temperature typically decreased by 20 to 30 K starting from ambient conditions.

4 RESULTS

4.1 General Flow Behavior

The data obtained with plateau experiments can be compared to the design values and computational fluid dynamics (CFD) calculations that were performed according to the experimental total conditions. For these numerical simulations, the DLR TAU code [12] was used. The Reynolds averaged Navier–Stokes equations were solved on a quasi-two-dimensional hybrid mesh. The full turbulent flow was computed with the Spalart–Allmaras model due to previous good experience for nozzle flows with this model [13, 14]. Local grid refinement was

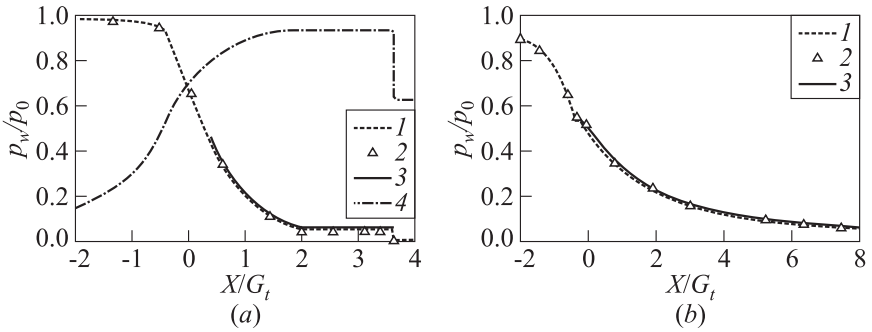

Figure 5 Comparision of CFD (*1*), experiment (*2*), and design (*3*): (*a*) pintle and center body; and (*b*) upper contour. Curve *4* shows the pintle geometry

used for higher resolution of the flow field inside and shortly downstream the nozzle. Around the nozzle, a far-field boundary with ambient conditions was used. The y^+ at the adiabatic walls was around 1.

The experimental values, taken from the stationary flow on pressure plateaus, were averaged over a minimum of 1 s and normalized by the total pressure. In Fig. 5*a*, the pintle and center body shapes are additionally plotted. In the convex part of the pintle, the pressure is seen to decrease rapidly, because the flow is expanded and, therefore, accelerated along the wall. The acceleration ends at the linear part of the center body; hence, no further pressure drop is observed. Both the numerical and experimental data show a lower pressure than would be expected from the design, especially along the center body. The mismatch of the assumed sonic line leads to additional expansion which could emanate from the contour wall.

In Fig. 5*b*, a comparison is made for the upper contour wall. In general, a good agreement can be found, but again the numerical results show a slightly higher expansion along the contour. The small delay in the expansion at the change from the wall circular arc to the upper wall contour profile indicates a failure in the design of those contour changes and needs improvement.

The incoming pressure on the upper contour side (at the axial position $X/G_t = -2.0$) is lower than that on the pintle. Due to the pintle shape, the flow is slower near the concave wall as on the upper contour side it is continuously accelerated.

4.2 Base Pressure and Flow Transition

The pressure at the center body base (p_b) was measured statically at two positions with a distance of $0.41G_t$ and $0.81G_t$ from the centerline, respectively.

The difference between the two gauge signals was within the measurement uncertainty; thus, p_b was presented as the mean value of both sensors.

With the plateau-type test profiles, the experience on flow transition was gained at stationary conditions and with coarse resolution. According to Fig. 6, the transition between open and closed-wake modes takes place between NPR 20 and 23.2. With increasing the NPR, the base pressure decreases as a result of the aspiration effect of the recirculation zone. The shear layer turns to the centerline due to the expansion around the center body corner. Thus, the supersonic flow region widens with the total pressure, but the recirculation zone downstream the center body becomes, therefore, shorter. Thus, the recirculating flow accelerates, the aspiration effect is intensified, and the base pressure drops. In the closed-wake mode, the recirculation zone becomes a trapped vortex and the connection to the ambience is cut. From now on, the pressure in the vortex is linked to the supersonic flow. As a result, the base pressure changes its trend and increases with further increasing NPR.

A more detailed view of the transition process is given by the plot of the base pressure variation during a single up- and downramping in Fig. 6. Like for the plateau-type profiles, the base pressure decreases with increasing NPR. A steeper gradient is visible just before the transition. The gradient of the nozzle pressure ratio is $d\mathrm{NPR}/dt = 0.5$. The actual transition is characterized by a two-third decrease in the base pressure within 50 ms. At higher NPRs, the base pressure increases as it is decoupled from the ambience and the aspiration effect is absent. The base region with the trapped vortex is further compressed only by the supersonic flow expanding around the base corner.

Thus, on the downramping profile, if the NPR has a negative gradient, the behavior of the base pressure differs from that on the upramping profile. The deviation occurs from the transition point at around NPR = 21.8 onwards. Here, the minimum base pressure of $p_b/p_a = 0.25$ is attained. However, with further lowering of the NPR, it increases again. Even a small jump of $\Delta p_b/p_a = 0.05$ at around NPR = 21.25 can be found. This first aberration is present in all base pressure distributions, but the shape is not always that strong as in the presented test results. After this small pressure rise, the base pressure acts like in the open-wake mode, because the base pressure reacts opposite to the NPR. It is interesting to note that the pressure downstream of the redirected shock wave (see Fig. 1*a*) does not show this behavior. It further decreases until the retransition point. The retransition takes place at NPR = 18.2, also with a duration of 50 ms. The base pressure jumps back to the pressure value of the open-wake mode. Thus, on the downramping profile, the situation between the transition and retransition points cannot be described by the flow feature of a closed-wake mode due to the opposite behavior of the base pressure. The obvious hysteretic effect needs further studies on the effect of condensation as it was observed by Mueller and Hall [15] and on the effect of the wall at the centerline which substitutes the symmetry line.

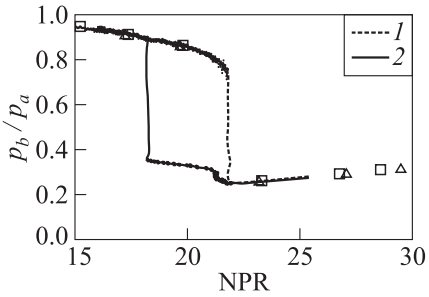

Figure 6 Base pressure distribution, open-to-close transition: *1* — upramping; *2* — downramping; signs — experiments

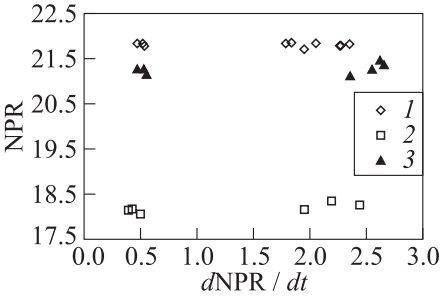

Figure 7 Transition behavior at different NPR gradients: *1* — transition; *2* — retransition; and *3* — first deviation

In Fig. 7, the transition and retransition NPR are plotted vs. the absolute gradient of the NPR. The number of transition experiments exceeds the number of retransitions, because data from the plateau-profile tests were also used. For those tests, the retransition occurred during the shutdown process and proper test conditions cannot be assured. All data were taken at the beginning of the sudden change in the wall pressure distribution. As mentioned before, the transition occurred in about 50 ms. However, both the transition and the retransition data show a very small difference between the test runs. Additionally, no influence of the ramping gradient was found.

The first deviation, i. e., the first sudden pressure rise, without retransition in the base pressure profile during downramping is indicated in Fig. 7 by triangular symbols. It occurs at NPR = 21.25 with a tendency to begin at slightly higher pressure ratios at larger gradients.

4.3 Off-Design Flow

Although the area of application of present-day ED nozzles would be in upper stage engines or in moon/planet soft-landing missions, which means almost or full vacuum conditions at the exit, understanding of the flow field at very low pressure ratios is needed for ground testing. This is because the first experiments of a scaled ED nozzle would be run at test facilities working under ambient conditions. Under these conditions, very low NPRs are passed during the transient startup and shutdown processes and the related flow field behavior is far from the design point. The flow behavior could include separation, causing side loads and undesirable shock interaction.

Therefore, tests at off-design conditions were performed, varying the NPR between 2.5 and 10 with different gradients. Under these test conditions, flow

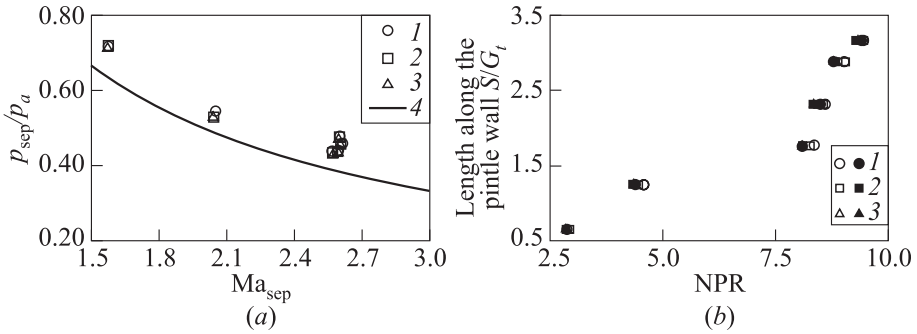

Figure 8 Flow separation at low NPRs: (*a*) separation positions on the center body compared to the criterion of Stark and Wagner [16]; and (*b*) separation positions along the center-body wall: *1* — $d\mathrm{NPR}/dt = 3.0$; *2* — 1.0; *3* — $d\mathrm{NPR}/dt = 0.25$ (black signs refer to negative meanings of $d\mathrm{NPR}/dt$); and *4* — separation criterion

separation was observed on the center body. In Fig. 8*a*, the position of the separation is plotted vs. the resulting Mach number ($\mathrm{Ma}_{\mathrm{sep}}$) for the separation pressure (p_{sep}). The separation position was determined by the sudden change in the pressure distribution caused by the moving separation front. Thus, the data are limited to pressure port positions. For the sake of clarity, the separation data are presented only for the upramping profiles and for different NPR gradients. It has been averaged over several tests. The concentration of points at $\mathrm{Ma}_{\mathrm{sep}} = 2.6$ is related to the pressure ports on the straight center-body wall where the flow is not further accelerated, but the movement of the separation front along this wall can still be measured.

Included in Fig. 8*a* is the criterion suggested by Stark and Wagner [16], where $p_{\mathrm{sep}}/p_a = 1/\mathrm{Ma}_{\mathrm{sep}}$, that is valid for turbulent separation in bell-type nozzles. The data show comparatively higher separation pressures, like it can be found for planar nozzles in the literature [17].

Figure 8*b* clarifies the movement of the separation along the center-body wall. The separation position is plotted for the actual length along the wall. At the change from the pintle circular arc to the straight center body, the third pressure port is located at $1.7S/G_t$. The separation is delayed just in front of this position, since a large gap in the separation profile between NPR = 4.5 and 8.0 exists. The separation which occurs along the center-body wall generates a separation shock. This causes flow interaction at the upper contour which is visible in its wall pressure distribution in Fig. 9. The wall pressure is normalized by the ambient pressure and plotted along the upper contour length for different NPRs. The array of curves has an offset according to the NPR in the undisturbed region. The discrepancy from the vacuum profile takes place depending on the NPR around $p_w/p_a = 1.0$ for low NPR, down to $p_w/p_a = 0.7$ for higher NPRs. The

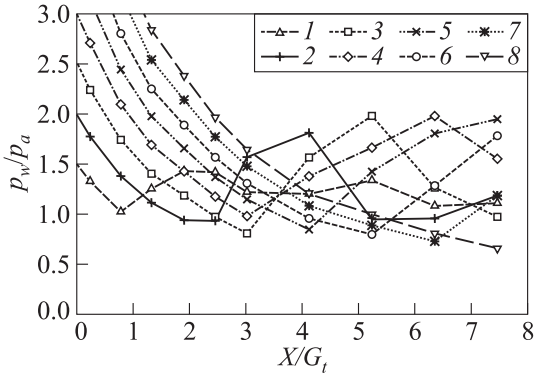

Figure 9 Pressure distribution along the upper contour at low NPRs: *1* — 3; *2* — 4; *3* — 5; *4* — 6; *5* — 7; *6* — 8; *7* —9; and *8* — 10

flow is recompressed at the upper contour due to interaction with the separation shock coming from the center body. The interaction could either be an ordinary shock reflection or shock reflection with a separation zone. Future tests using Schlieren optics will clarify this effect. Note that the upper contour pressure is recompressed up to $p_w/p_a = 2$ for NPR = 5, but drops to 1.1 of the ambient pressure at the nozzle exit. For NPR = 7.0, no expansion after the pressure rise is visible, because it is too close to the nozzle exit. As the exit pressure is always above the ambient pressure, normal flow separation can be excluded, because in this case, the region behind the separation shock would be dominated by the ambient pressure. At NPR = 10, no discrepancy from the vacuum profile can be found anymore. This corresponds to the previous findings (see Fig. 8*b*) that the last measured separation occurs at NPR around 9.

5 SUMMARY AND OUTLOOK

A planar ED nozzle was tested at the cold-flow P6.2 test bench. Experiments under design and off-design conditions were performed. The transition between open and closed-wake modes was observed and a hysteretic effect was found. With decreasing NPR, the base pressure behaves opposite to the expected decrease. At very low NPRs, flow separation occurs on the center body. The separation is delayed at the end of the convex pintle part and moves along the center body. The separation behavior is independent of the NPR gradient. Accompanying numerical simulations are ongoing and will be validated against the experimental results.

The presented experiments are a part of the ED test program at DLR Lampoldshausen. The next steps are tests with optical diagnostics through window

segments. Despite the throat and the base region are of major interest, the whole flow field will be observed. In addition to the Schlieren optics, the wake closure and opening will be studied in more detail with sidewall pressure measurements.

Future tests at M11 test bench are also planned. An air heater will be used to provide hot (up to 1300 K) humid air for further temperature-dependent investigations. The nozzle will then be equipped with thermocouples around the throat region.

ACKNOWLEDGMENTS

The test bench was operated by C. Böhm, and his help and support are appreciated.

REFERENCES

1. Rao, G. 1960. The E-D nozzle. *Astronautics*. 28–29, 50–51.
2. Wasko, R. 1968. Performance of annular plug and expansion-deflection nozzles including external flow effects at transonic Mach numbers. NASA TN D-4462.
3. Goetz, A., G. Hagemann, J. Kretschmer, and R. Schwane. 2005. Advanced upper stage propulsion concept — the expansion-deflection upper stage. AIAA Paper No. 2005-3752.
4. Lentsch, A., and V. Leudiere. 2002. Performace estimation of an expander bleed cycle. *4th Conference (International) on Laucher Technology*. Liege.
5. Taylor, N. 2002. An integrated approach to expansion deflection nozzle analysis. Ph.D. Thesis. University of Bristol.
6. Taylor, N., and C. Hempsell. 2004. Throat flow modelling of expansion deflection nozzles. *J. Brit. Interplanetary Soc.* 57:242–50.
7. Sauer, S. 1947. General characteristics of the flow through nozzles at near critical speeds. NACA TM-1147. Reprint.
8. Kronmüller, H., and K. Schäfer. 2002. Cold gas subscale test facility P6.2 at DLR Lampoldshausen. *6th Symposium (International) for Space Transportation of the XXI Century*. Versailles.
9. Schäfer, K., C. Böhm, H. Kronmüller, R. Stark, and H. Zimmermann. 2005. P6.2 cold gas test facility for simulation of flight conditions — current activities. *1st European Conference for Aerospace Sciences*. Moscow.
10. Börger, G. 1973. Optimierung von Windkanaldüsen für den Unterschallbereich. Ph.D. Thesis. Fakultät für Maschinenbau und Konstruktiven Ingenieurbau, Ruhr-Universität Bochum.
11. Mueller, T., and C. Hall. 1968. Separated flow region within a planar expansion-deflection nozzle. *J. Spacecraft* 5:738–40.

12. Mack, A., and V. Hannemann. 2002. Validation of the unstructured DLR-TAU-code for hypersonic flows. AIAA Paper No. 2002-3111.
13. Stark, R., and B. Wagner. 2006. Experimental flow investigation of a truncated ideal contour nozzle. AIAA Paper No. 2006-5208.
14. Stark, R., and G. Hagemann. 2007. Current status of numerical flow prediction for separated nozzle flows. *2nd European Conference for Aerospace Sciences*. Brussel.
15. Mueller, T., and C. Hall. 1968. On the separated flow region within a planar expansion-deflection nozzle. AIAA Paper No. 68-82.
16. Stark, R., and B. Wagner. 2009. Experimental study of boundary layer separation in truncated ideal contour nozzles. *Shock Waves* 19:185–91.
17. Lawrence, R. 1967. Symmetrical and unsymmetrical flow separation in supersonic nozzles. Ph.D. Thesis. Institute of Technology of Southern Methodist University. NASA CR 92587.